Improved quantitative description of Auger recombination in crystalline silicon

Armin Richter[*] and Stefan W. Glunz

Fraunhofer Institute for Solar Energy Systems (ISE), Heidenhofstrasse 2, 79110 Freiburg, Germany

Florian Werner and Jan Schmidt

Institute for Solar Energy Research Hameln (ISFH), Am Ohrberg 1, 31860 Emmerthal, Germany

Andres Cuevas

Research School of Engineering, The Australian National University, Canberra, ACT 0200, Australia
(Received 28 March 2012; revised manuscript received 11 June 2012; published 9 October 2012)

An accurate quantitative description of the Auger recombination rate in silicon as a function of the dopant density and the carrier injection level is important to understand the physics of this fundamental mechanism and to predict the physical limits to the performance of silicon based devices. Technological progress has permitted a near suppression of competing recombination mechanisms, both in the bulk of the silicon crystal and at the surfaces. This, coupled with advanced characterization techniques, has led to an improved determination of the Auger recombination rate, which is lower than previously thought. In this contribution we present a systematic study of the injection-dependent carrier recombination for a broad range of dopant concentrations of high-purity *n*-type and *p*-type silicon wafers passivated with state-of-the-art dielectric layers of aluminum oxide or silicon nitride. Based on these measurements, we develop a general parametrization for intrinsic recombination in crystalline silicon at 300 K consistent with the theory of Coulomb-enhanced Auger and radiative recombination. Based on this improved description we are able to analyze physical aspects of the Auger recombination mechanism such as the Coulomb enhancement.

I. INTRODUCTION

Band-to-band Auger recombination processes are a generalization of the atomic Auger effect: An electron recombines with a hole and the excess energy is transferred to another free charge carrier. With improved device technology, i.e., surface passivation, Auger recombination has become increasingly important for the performance of silicon devices, e.g., bipolar transistors[1,2] or silicon solar cells.[3,4] Since Auger recombination is an intrinsic property of silicon, it ultimately limits device performance, unlike defect recombination, which can be reduced by avoiding defects. While the carrier lifetime in lowly doped silicon is mainly affected by the Auger mechanism under high-injection conditions,[5] the carrier lifetime in highly doped silicon is also affected under low-injection conditions.[1,6]

The excess energy of the Auger recombination processes is either transferred to another electron ("eeh" process) or hole ("ehh" process). Traditionally, the charge carriers involved in these purely collisional Auger processes are assumed to be noninteracting quasifree particles.[7–9] As a result, the recombination rates of both processes, R_{eeh} and R_{ehh}, are proportional to the involved carrier densities: $R_{eeh} = C_n n^2 p$ and $R_{ehh} = C_p n p^2$, where n and p are the electron and hole densities, and C_n and C_p are the respective Auger coefficients. The total Auger recombination rate R_{Auger} is then the sum of R_{eeh} and R_{ehh}. From this traditional Auger theory, the Auger lifetimes can be approximated for high-injection conditions to

$$\tau_{Auger,hi} = \frac{1}{(C_n + C_p)\Delta n^2} = \frac{1}{C_a \Delta n^2},\qquad(1)$$

and for low-injection conditions to

$$\tau_{Auger,li} = \frac{1}{C_n N_{dop}^2} \quad \text{for } n\text{-type silicon, and}\qquad(2)$$

$$\tau_{Auger,li} = \frac{1}{C_p N_{dop}^2} \quad \text{for } p\text{-type silicon,}\qquad(3)$$

where $\Delta n = n - n_0 = p - p_0$ is the excess carrier density, n_0 and p_0 are the thermal equilibrium concentrations of electrons and holes, N_{dop} is the net dopant concentration, and $C_a \equiv C_n + C_p$ is the ambipolar Auger coefficient. Thus, in high-injection conditions τ_{Auger} is only a function of Δn, while under low-injection conditions it depends only on N_{dop}. The most cited values of the Auger coefficients are those of Dziewior and Schmid[10] with $C_n = 2.8 \times 10^{-31}$ cm^6 s^{-1} and $C_p = 9.9 \times 10^{-32}$ cm^6 s^{-1}. Sinton and Swanson accurately measured C_a in the Δn range between 10^{15} and 2×10^{17} cm^{-3}, which was found to be 1.66×10^{-30} cm^6 s^{-1} and thus about four times higher than the sum of C_n and C_p.[11]

This traditional Auger theory is in good agreement with measured lifetimes of highly doped silicon ($N_{dop} > 5 \times 10^{18}$ cm^{-3}). For lower dopant concentrations, however, the predicted lifetimes significantly exceed the measured lifetimes.[10] Hangleiter and Häcker attributed this deviation to Coulomb interactions of mobile charge carriers, by applying a quantum-mechanical theory to lowly injected silicon.[12] According to this theory, the correlated charge carriers form bound states (i.e., excitons) and scattering states. Due to the formation of excitons, the electron density in the vicinity of a hole is increased, which consequently increases the Auger recombination probability. At high majority carrier densities

the exciton formation can be described by a Mott transition: For majority carrier densities above the excitonic Mott density (for silicon approximately 1×10^{18} cm^{-3} at 300 K)[6] the exciton formation is strongly suppressed due to screening of the electron-hole interaction. Thus, this Coulomb-enhanced Auger recombination (CE-AR) converges to the traditional Auger recombination of noninteracting charge carriers. To account for CE-AR, the Auger coefficients C_n and C_p are multiplied with the enhancement factors g_{eeh} and g_{ehh}, respectively.[12] Based on lifetime measurements Altermatt *et al.* proposed an empirical parametrization of g_{eeh} and g_{ehh} for low-injection conditions:[6]

$$g_{eeh}(n,T)$$
$$= 1 + [g_{max,n}(T) - 1]\left\{1 - \tanh\left[\left(\frac{n}{N_{0,eeh}}\right)^{0.34}\right]\right\}, \quad (4)$$

$$g_{ehh}(p,T)$$
$$= 1 + [g_{max,p}(T) - 1]\left\{1 - \tanh\left[\left(\frac{p}{N_{0,ehh}}\right)^{0.29}\right]\right\}, \quad (5)$$

where $g_{max,n} = g_{max,p} = 45$ at 300 K, and $N_{0,eeh} = N_{0,ehh} = 5 \times 10^{16}$ cm^{-3}.

In addition to the Coulomb interactions, the Auger recombination processes can occur also with phonon participation[13,14] or involve impurities.[15] For a fundamental understanding of the involved processes, theoretical models are indispensable, as Auger recombination cannot be determined directly, like radiative recombination.[16] However, a theoretical determination of the Auger recombination rate as a function of the dopant density and the excess carrier density is not yet possible, as not all involved processes are completely understood.[13,14] Thus, for a quantitative description empirical parametrizations based on the equations of the traditional Auger theory are used.[17–21] A review of the various parametrizations can be found in Ref. 21. Widely used is the parametrization proposed by Kerr and Cuevas in 2002 for silicon at 300 K.[21] They included the radiative recombination according to Schlangenotto *et al.*[22] in their parametrization, so that the predicted intrinsic lifetime of silicon reads

$$\tau_{intr,Kerr} = \frac{\Delta n}{np\left(C_n^* n_0^{0.65} + C_p^* p_0^{0.65} + C_a^* \Delta n^{0.8} + B^*\right)}, \quad (6)$$

with $C_n^* = 1.8 \times 10^{-24}$, $C_p^* = 6 \times 10^{-25}$, $C_a^* = 3 \times 10^{-27}$, and $B^* = 9.5 \times 10^{-15}$.

Such empirical parametrizations are based on experimentally determined minority carrier lifetime data where the surface recombination is neglected. Hence, the accuracy of these empirical parametrizations is limited by the quality of surface passivation. Over the last years, silicon surface passivation has improved continuously. In particular, Al$_2$O$_3$ appeared to feature extremely low surface recombination velocities (SRV) below 5 cm/s,[23–27] which allows for investigating silicon bulk recombination with a high precision. Recently, several authors have reported measured effective lifetime values for lowly doped silicon exceeding Kerr's intrinsic lifetime limit.[25,28,29] This indicates that it is necessary to revise the quantitative description of the Auger recombination. Meanwhile, the description of the radiative recombination coefficient B in silicon has also been improved: Trupke *et al.*

measured thoroughly B as a function of the temperature,[30] which appeared to be 50% smaller than the value measured by Schlangenotto *et al.* at 300 K. Subsequently, Altermatt *et al.* introduced a B model, which accounts for Coulomb interaction of electrons and holes.[31] At the same time, the lifetime measurement techniques were developed further, too.[32–34]

Based on the improved surface passivation techniques for silicon wafers, particularly by depositing Al$_2$O$_3$ and SiN$_x$, we examine the Auger recombination as a function of the injection level and the dopant density for lowly doped silicon very accurately in this work. Therefore, we measure the injection-dependent effective recombination lifetime of passivated p-type and n-type silicon wafers with various dopant densities. To assess the accuracy of our effective lifetime measurements, we first compare two independent measurement techniques at two different laboratories. Based on these experimental lifetime results, we introduce a parametrization for the intrinsic lifetime of crystalline silicon at 300 K, which is consistent with the theory of CE-AR, accounts for Coulomb-enhanced radiative recombination, and permits the quantification of Auger recombination for a broad range of dopant concentrations and excess carrier densities.

II. EXPERIMENTS

A. Sample preparation

To study the intrinsic recombination of crystalline silicon (c-Si) as a function of the excess carrier density and the dopant concentration, symmetrical passivated lifetime samples have been prepared in parallel at Fraunhofer ISE and at ISFH using different surface passivation equipment and procedures. Due to this parallel processing systematic errors can be considerably reduced.

Shiny-etched phosphorus-doped n-type and boron-doped p-type float-zone (FZ) silicon wafers, as well as some phosphorus-doped n-type Czochralski (Cz) silicon wafers were used as base material. All wafers feature a (100)-oriented surface and the wafer thickness ranges from 180 to 300 μm. The wafer dopant concentration ranged between 4.6×10^{13} cm^{-3} and 2.5×10^{17} cm^{-3}. For a controlled variation of the wafer thickness, some wafers were mechanically thinned using a grinder.[35] The grinding damage on the wafer surface was removed by a chemical polishing solution. At Fraunhofer ISE, the wafer surface was cleaned in a HNO$_3$ solution, followed by a dip in diluted HF prior to the deposition of the passivating layers. The samples were either passivated with Al$_2$O$_3$ or with a-SiN$_x$:H (briefly SiN$_x$). Plasma-assisted atomic layer deposition (PA-ALD) in a commercial ALD reactor (OpAL, Oxford Instruments) was used to deposit the Al$_2$O$_3$ layers. Typically, the deposition was performed at a substrate temperature of 180 °C. After the deposition of ∼30-nm-thick Al$_2$O$_3$ layers, the samples were annealed at 440 °C for 25 min in forming gas ambient (N$_2$/H$_2$), to activate the surface passivation of Al$_2$O$_3$. The 70-nm-thick SiN$_x$ layers were deposited via plasma-enhanced chemical vapor deposition (PECVD) using a reactor with a microwave induced plasma (AK800, Roth & Rau). At ISFH the wafers were cleaned according to the standard RCA procedure[36] and

afterwards passivated with 10-nm-thick Al_2O_3 layers. The Al_2O_3 layers were deposited using PA-ALD in a FlexAL reactor from Oxford Instruments. To activate the surface passivation of the Al_2O_3 layers, the samples were annealed afterwards at 425 °C for 15 min in nitrogen gas ambient.

B. Characterization techniques

The effective minority carrier lifetime τ_{eff} was measured using the photoconductance decay (PCD) technique as well as the photoluminescence (PL) technique. In the case of the PCD technique, the decay of Δn generated by a short illumination is determined from the measured decay of the excess photoconductance $\Delta\sigma$, which is directly related to Δn:[37–39]

$$\Delta\sigma = e\Delta n(\mu_n + \mu_p)W, \tag{7}$$

with the elementary charge e, the wafer thickness W and the electron and hole mobility μ_n and μ_p, respectively. For silicon, the variation of the carrier mobility with the carrier concentrations is well known;[40–43] thus Eq. (7) can be solved iteratively to find Δn for each measured $\Delta\sigma$.[44] The PCD measurements were performed with the lifetime tester WCT-120 from Sinton Instruments. This tool illuminates the sample with a white light flash lamp and the samples' photoconductance decay is measured contactless with a calibrated rf bridge circuit, which is inductively coupled to the samples' conductivity.[39,45] The light intensity of the flash lamp is measured with a calibrated concentrator solar cell simultaneously with the voltage signal of the rf bridge circuit. The PCD measurements were either performed in the transient mode[5,37,38] (tr-PCD) or in the quasi-steady-state mode (QSSPC) using a generalized analysis.[46] In tr-PCD, the decay of $\Delta\sigma$ is measured *after* the excess carrier generation by the short light pulse is terminated. τ_{eff} is then determined directly from the time-dependent decay of $\Delta n(t)$:

$$\tau_{eff}[\Delta n(t)] = -\frac{\Delta n(t)}{d\Delta n(t)/dt}. \tag{8}$$

However, the determination of low τ_{eff} values with tr-PCD require a fast PCD measurement and also a fast decaying light pulse. For the WCT-120 tool with a minimum flash lamp decay time of $\sim 30\ \mu s$, tr-PCD measurements are limited to samples with τ_{eff} above $\sim 200\ \mu s$. In particular, samples with lower lifetime values were measured in the QSSPC mode. In this mode the sample is illuminated with a prolonged light pulse, featuring an exponential decay with a time constant of 2.1 ms. For these quasi-steady-state measurement conditions, the continuity equation can be written as[46]

$$\tau_{eff}[\Delta n(t)] = \frac{\Delta n(t)}{G(t) - d\Delta n(t)/dt}, \tag{9}$$

with the photogeneration rate $G(t)$. To calculate τ_{eff} from this generalized analysis of QSSPC measurements, $G(t)$ is required, which is determined from the calibrated voltage signal of the concentrator solar cell. It is worth mentioning that the effective lifetime determined from PCD measurements in both the tr-PCD mode and the QSSPC mode does not depend on the depth profile of the minority carrier distribution, except for the weak dependence introduced by evaluating the mobility for an averaged carrier concentration.[39,46] However, even for

the varying absorption depth of the white light flash lamp, the carrier concentration is homogeneous throughout the wafer thickness, as the samples are much thinner than the diffusion length. This holds for all samples measured within this work, except for the p-type samples with N_{dop} above 10^{17} cm^{-3}. It is important to note that lifetime measurements with the lifetime tester WCT-100 can result in significant uncertainties for N_{dop} below $\sim 5 \times 10^{14}$ cm^{-3}.[33,47] We observed this with our WCT-120 setup too, when measuring samples with N_{dop} below $\sim 5 \times 10^{13}$ cm^{-3}. To gain more confidence for the results, all samples with N_{dop} below $\sim 5 \times 10^{14}$ cm^{-3} were measured with the PL technique.

The PL technique monitors the Δn decay by measuring the time-dependent light emitted by the radiative recombination of electrons and holes. The relation between the photoluminescence intensity I_{PL} of the radiative recombination and Δn is given by[32,34,48]

$$I_{PL} = AB\Delta n(\Delta n + N_{dop}), \tag{10}$$

with the radiative recombination coefficient B. The factor A accounts for optical properties of the measurement setup and the sample. The PL measurements are carried out with a setup where the samples are illuminated from the top side either with a light emitting diode (LED) array or a beam-shaped laser, with a wavelength of 810 and 790 nm, respectively. The photoluminescence is measured with a photodetector placed below the sample. The illumination light intensity is monitored with a second, calibrated photodetector to determine $G(t)$. Some PL measurements were performed under quasi-steady-state conditions (QSSPL) applying the self-consistent calibration proposed by Trupke et al.[32] By applying a suitably chosen intensity shape of the light pulse (featuring a slow rise *and* a slow decay) the continuity equation under quasi-steady-state conditions, given in Eq. (9), can be used to determine a self-consistent value for the calibration factor A, as required for the determination of $\Delta n(t)$ from Eq. (10).[32] Alternatively, PL measurements were also performed under steady-state conditions (SSPL) as described by Giesecke et al., which makes use of a self-consistent QSSPL measurement as a lifetime calibration, i.e., to determine the factor A which is then also used for SSPL.[34] In the case of SSPL, τ_{eff} is determined from the steady-state relation $\tau_{eff} = \Delta n/G$, which is not a dynamic measurement such as QSSPL, QSSPC, and tr-PCD. Therefore, the sample is illuminated with sufficiently long, square-shaped laser light pulses, with typical modulation frequencies between 1 and 100 Hz. Depending on the signal-to-noise ratio, the SSPL measurements are repeated and averaged over a sufficient number of modulation periods. For both PL methods, the evaluation of the effective lifetime depends on the radiative recombination coefficient B, which is a function of the mobile charge carrier density, i.e., Δn and N_{dop}, due to Coulomb interactions at high carrier concentrations.[31] This was taken into account according to the parametrization given in Ref. 49, which is based on quantum-mechanical modeling of the radiative recombination including Coulomb interactions. It should also be mentioned that τ_{eff} resulting from PL measurements can be affected by reabsorption processes, when Δn varies strongly perpendicular to the wafer surface.[50,51] Trupke pointed out, however, that for $\tau_{eff} > 50\ \mu s$ this effect is negligible.[50] This is fulfilled for all our samples measured with

TABLE I. Details of the wafers prepared in this work for the dopant concentration variation. From the maximum measured lifetime of each sample, the maximum surface recombination velocity $S_{eff,max}$ was estimated with Eq. (11) assuming an infinite bulk lifetime. The last two columns show the recombination current density prefactors J_0 and the ideality factors m, which were used to model the surface depletion region recombination of those samples according to Eq. (16).

Sample No.	Dopant type	Growth method	ρ_{bulk}[a] (Ω cm)	N_{dop} (cm^{-3})	W (μm)	Passivation layer	Max. τ_{eff} (ms)	$S_{eff,max}$ (cm/s)	τ_{eff} measurement method	J_0 (nA/cm^{-3})	m
#1	n	FZ	95	4.7×10^{13}	203	Al$_2$O$_3$[b]	22	0.5	QSSPL	46	4.0
#2	n	FZ	97	4.6×10^{13}	203	Al$_2$O$_3$[b]	32	0.3	SSPL	23	3.8
#3	n	FZ	10.3	4.4×10^{14}	204	Al$_2$O$_3$[b]	27	0.4	SSPL	30	3.8
#4	n	FZ	1.56	3.1×10^{15}	239	Al$_2$O$_3$[c]	9.3	1.3	PCD	–	–
#5	n	FZ	0.96	5.2×10^{15}	203	Al$_2$O$_3$[b]	4.3	2.4	QSSPL	76	4.0
#6	n	FZ	1.00	4.9×10^{15}	181	Al$_2$O$_3$[b]	6.8	1.3	SSPL	20	3.8
#7	n	FZ	1.00	4.9×10^{15}	200	SiN$_x$[d]	6.3	1.6	QSSPL	–	–
#8	n	Cz	0.41	1.3×10^{16}	197	SiN$_x$[d]	1.2	8.6	PCD	–	–
#9	p	FZ	100	1.3×10^{14}	254	Al$_2$O$_3$[b]	33	0.4	QSSPL	–	–
#10	p	FZ	105	1.3×10^{14}	253	Al$_2$O$_3$[b]	40	0.3	SSPL	–	–
#11	p	FZ	9.7	1.4×10^{15}	256	Al$_2$O$_3$[b]	13	1.0	QSSPL	–	–
#12	p	FZ	9.8	1.4×10^{15}	253	Al$_2$O$_3$[b]	19	0.7	SSPL	–	–
#13	p	FZ	1.34	1.1×10^{16}	303	Al$_2$O$_3$[c]	3.7	4.1	QSSPL, PCD	–	–
#14	p	FZ	1.26	1.2×10^{16}	300	Al$_2$O$_3$[c]	6.8	2.2	PCD	–	–
#15	p	FZ	1.00	1.5×10^{16}	250	Al$_2$O$_3$[b]	3.1	4.0	QSSPL	–	–
#16	p	FZ	1.05	1.4×10^{16}	250	Al$_2$O$_3$[b]	3.9	3.2	PCD	–	–
#17	p	FZ	0.49	3.3×10^{16}	297	Al$_2$O$_3$[c]	0.95	15.6	PCD	–	–
#18	p	FZ	0.47	3.4×10^{16}	251	Al$_2$O$_3$[b]	0.87	14.5	QSSPL	–	–
#19	p	FZ	0.16	1.3×10^{17}	259	Al$_2$O$_3$[c]	0.088	147	PCD	–	–
#20	p	FZ	0.10	2.5×10^{17}	255	Al$_2$O$_3$[b]	0.037	346	QSSPC	–	–

[a]Measured bulk resistivity of the wafers.
[b]Deposition technique: PA-ALD using OpAL reactor.
[c]Deposition technique: PA-ALD using FlexAL reactor.
[d]Deposition technique: PECVD.

PL, expect for the low-injection lifetime ($\Delta n < 10^{11}$ cm^{-3}) of the Al$_2$O$_3$ passivated n-type samples. For the evaluation of the SSPL measurements, actually, the reabsorption was taken into account as described in Ref. 34. All lifetime measurements were performed at a temperature of 300 ± 5 K.

For all lifetime measurement methods mentioned above, the knowledge of the wafer thickness W as well as N_{dop} is required. The wafer thickness was measured either with a contactless wafer geometry gauge (E + H Metrology) or with a dial indicator, with a relative accuracy of 1% resulting from comparison of both. To determine N_{dop}, four point probe measurements were performed and from the resulting bulk resistivity N_{dop} was calculated using the mobility model of Ref. 43. The accuracy of the determined N_{dop} is estimated to be 5%.

C. Uncertainty of the lifetime measurements

Before considering a quantitative description of the Auger recombination based on effective lifetime measurements, we first verified our effective lifetime measurements. Therefore, we compared independent lifetime measurement techniques at two different laboratories to exclude systematic deviations caused by specific measurement procedures: (i) PCD measured at ISFH and (ii) PCD as well as QSSPL measured at Fraunhofer ISE. An Al$_2$O$_3$-passivated p-type FZ silicon sample ($N_{dop} = 1.1 \times 10^{16}$ cm^{-3}) was used for this experiment (sample #13 in Table I). The resulting effective lifetime data are compared in Fig. 1. The upper graph shows the relative deviation of

both PCD measurements with respect to the PL measurement. As can be seen, all measurements are in good agreement. In particular, the relative deviation is below 10% for the injection range above 10^{15} cm^{-3}, the range dominated by Auger recombination. The decrease of the effective lifetime for $\Delta n < 10^{15}$ cm^{-3} indicates that the low-injection range is dominated by defect recombination. It is important to note that this agreement is observed for independent effective lifetime measurement techniques based on different detectors measuring either the illumination induced photoconductance decay (PCD) or the illumination induced decay of the spontaneous emission of the radiative recombination (PL). In addition, the evaluation of τ_{eff} also involves different material parameters: for PCD particularly the carrier mobility, and for PL mainly the radiative recombination coefficient, both as a function of the mobile carrier concentration. Thus, the good agreement of τ_{eff} resulting from PCD and PL demonstrates also the robust and consistent extraction of both Δn as well as τ_{eff}, and particularly in the relevant injection range for Auger recombination. From these lifetime comparison measurements as well as the measurement uncertainties, we estimated a relative uncertainty range of $\pm 20\%$ for lifetime measurements carried out within this work (dashed gray lines in the upper graph of Fig. 1). This uncertainty range accounts for the uncertainty in the extracted τ_{eff} and also in Δn.

Figure 1 also compares the measured lifetime data with $\tau_{intr,Kerr}$ according to Eq. (6). The relative deviation with respect to the PL measurement is plotted in the upper
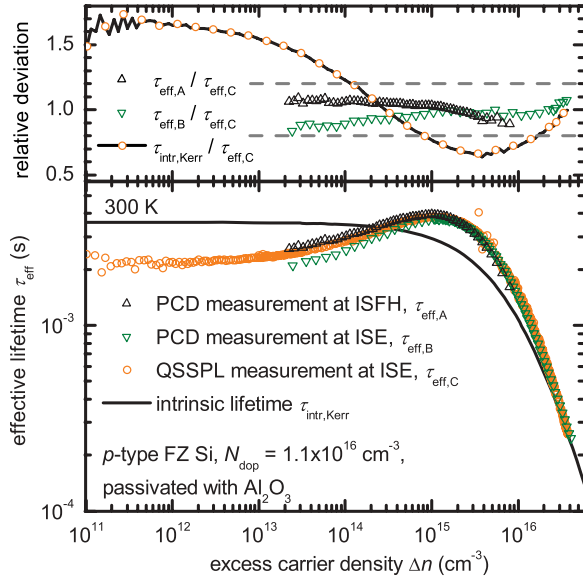
FIG. 1. (Color online) Comparison of different lifetime measurement techniques at different laboratories. The measurements were performed with an Al$_2$O$_3$-passivated p-type FZ Si sample ($N_{dop} = 1.1 \times 10^{16}$ cm^{-3}). The solid line represents $\tau_{intr,Kerr}$ after Eq. (6). The upper graph shows the relative deviations of the different τ_{eff} measurements with respect to the QSSPL measurement. The dashed lines mark the estimated uncertainty range of our τ_{eff} measurements.

graph. It can be seen that for $\Delta n > 5 \times 10^{14}$ cm^{-3} $\tau_{intr,Kerr}$ underestimates the measured effective lifetime considerably, with a maximum relative deviation of 36% for Δn around 3×10^{15} cm^{-3}. This deviation cannot be explained by lifetime measurement uncertainties.

III. RESULTS

A. Discrimination between bulk and surface recombination

In a first experiment, the bulk lifetime τ_{bulk} was determined for Al$_2$O$_3$-passivated p-type FZ Si samples with $N_{dop} = 1.4 \times 10^{16}$ cm^{-3} by applying the wafer thickness variation method[52] with mechanically thinned wafers. For symmetrically passivated samples, as used in this work, and for sufficient low surface recombination velocities S, the effective lifetime can be expressed as[53]

$$\frac{1}{\tau_{eff}} = \frac{1}{\tau_{bulk}} + \frac{2S}{W}, \tag{11}$$

with a relative accuracy of 4% for $SW/D < 0.25$, which is well fulfilled for the investigated samples. D is the diffusion constant of the excess carriers. This equation can be interpreted as a linear function of $1/W$ with a slope of $2S$ and an intercept of $1/\tau_{bulk}$. Hence, the contribution of bulk recombination and surface recombination on the measured effective lifetime can be separated by lifetime measurements on wafers with varying thickness. In this work, the slope and the intercept were calculated for each excess carrier density using linear regression. This is shown in Fig. 2 exemplarily for three different excess carrier densities.

The resulting τ_{bulk} and S are shown in Fig. 3 as a function of Δn, together with the measured effective lifetime of the samples used for the wafer thickness variation. The error bars
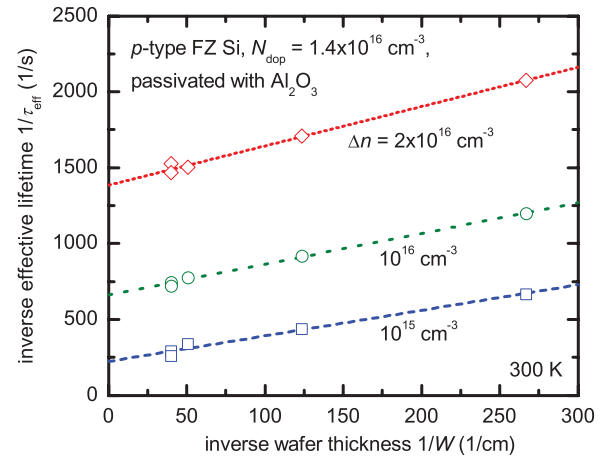

FIG. 2. (Color online) Plot of the inverse effective lifetime as a function of the inverse wafer thickness for Al$_2$O$_3$-passivated p-type FZ silicon samples with $N_{dop} = 1.4 \times 10^{16}$ cm^{-3} and wafer thicknesses between 38 and 250 μm. The data are shown exemplarily for three different excess carrier densities Δn.

of τ_{bulk} and S specify the uncertainty range resulting from the linear regression. For these Al$_2$O$_3$-passivated p-type samples ($N_{dop} = 1.4 \times 10^{16}$ cm^{-3}), a very low surface recombination level in the range of 1 cm/s is observed, in combination with a bulk lifetime as high as 4.5 ± 0.5 ms at Δn around 10^{15} cm^{-3}. In low injection, the measured effective lifetime decreases slightly. Since S exhibits a flat injection-independent value around 0.8 cm/s in this injection range, the decrease can
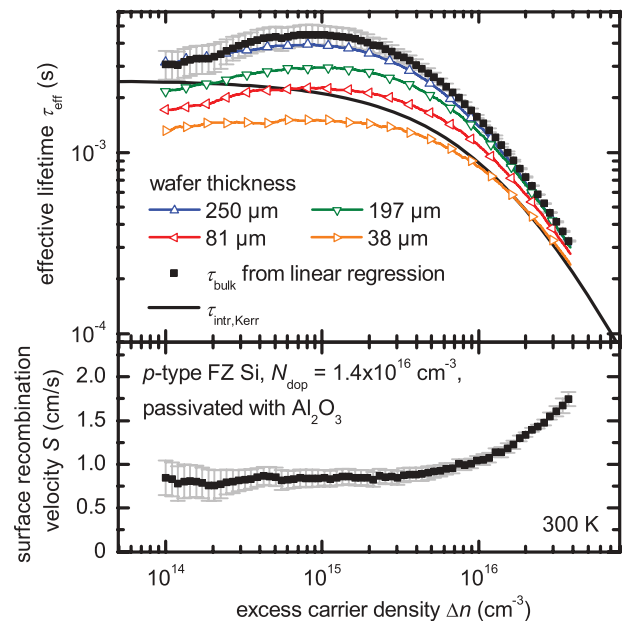

FIG. 3. (Color online) Measured effective lifetime for Al$_2$O$_3$-passivated p-type FZ Si samples with $N_{dop} = 1.4 \times 10^{16}$ cm^{-3} and wafer thicknesses between 38 and 250 μm. From this wafer thickness variation the silicon bulk lifetime τ_{bulk} and the surface recombination velocity S were calculated according to Eq. (11) by linear regression for each Δn. The error bars of τ_{bulk} and S indicate the uncertainty range resulting from the regression. The solid line is the intrinsic lifetime limit $\tau_{intr,Kerr}$ according to Eq. (6).

be clearly attributed to τ_{bulk}, and thus indicates a weak bulk recombination even for these high-quality FZ silicon wafers. The comparison of τ_{bulk} with $\tau_{\text{intr,Kerr}}$ in Fig. 3 reveals again an underestimation of about 55% at Δn around 10^{15} cm^{-3}, which is significantly higher than our 20% uncertainty range.

B. Carrier recombination as a function of injection level

To investigate the Auger recombination rate over a wide range of conditions, p-type and n-type silicon samples with dopant concentrations N_{dop} ranging from 4.6×10^{13} to 2.5×10^{17} cm^{-3} were carefully characterized. For this purpose we used selected samples showing the highest measured carrier lifetimes from different experiments performed over a time frame of more than one year to exclude any technological or processing variability. Table I gives an overview of the main parameters of these samples.

Figure 4 shows the measured effective lifetime for two representative sets of samples. Effective lifetimes up to 32 ms were observed for the lowest-doped n-type sample ($N_{\text{dop}} = 4.6 \times 10^{13}$ cm^{-3}), and up to 40 ms for the lowest-doped p-type sample ($N_{\text{dop}} = 1.3 \times 10^{14}$ cm^{-3}). If these effective lifetimes were interpreted to be solely due to surface recombination, that is, if intrinsic recombination in silicon was deemed to be inexistent, an upper limit for the SRV $S_{\text{eff,max}}$ as low as 0.3 cm/s would be determined from Eq. (11) for both samples, as shown in Table I. This indicates that it is reasonable to, instead, assume that surface recombination is negligible in these samples and interpret the measured effective lifetimes as a close reflection of intrinsic recombination in silicon.

As predicted by the Auger recombination theory, the maximum measured effective lifetime strongly decreases with increasing N_{dop}, although it remains above 1 ms for $N_{\text{dop}} < 1.5 \times 10^{16}$ cm^{-3}. For each sample, the effective lifetime decreases at high carrier injection levels, again as expected

from the Auger recombination theory. It can also be noted in Fig. 4 that for most samples the measured effective lifetime decreases towards the left of the maximum, that is, towards very low carrier injection levels. Except for sample #12 ($N_{\text{dop}} = 1.4 \times 10^{15}$ cm^{-3}) all Al$_2$O$_3$-passivated p-type samples show only a slightly decreasing effective lifetime with decreasing injection. Sample #12 shows a stronger decreasing lifetime in low injection which seems to saturate at a level around 5 ms. Such a saturating lifetime in low injection is typical of a Shockley-Read-Hall[54,55] (SRH) defect recombination. This defect recombination could either originate from the bulk or from the surface, or from a mixture of both. In the previous section an injection-independent SRV in low injection was determined for the Al$_2$O$_3$ passivation of the p-type sample with $N_{\text{dop}} = 1.4 \times 10^{16}$ cm^{-3}. Thus, one would expect a bulk defect recombination to be present in sample #12. We modeled the low-injection lifetime of sample #12 for two prominent recombination-active impurities in p-type silicon:[56] iron, either interstitially dissolved or paired with boron,[57] and oxygen, which forms boron-oxygen pairs under illumination,[58,59] both well characterized in terms of defect level and recombination capture cross section.[60–63] By treating the defect density as a single fit parameter, it was not possible to describe the low-injection lifetime accurately, either with iron impurities or with boron-oxygen pairs.

In contrast to the Al$_2$O$_3$-passivated p-type samples, the Al$_2$O$_3$-passivated n-type samples show a considerably stronger decrease of the effective lifetime in low injection. In the case of the n-type sample with $N_{\text{dop}} = 4.4 \times 10^{14}$ cm^{-3}, the effective lifetime drops over three orders of magnitude from about 30 ms at $\Delta n \sim 10^{15}$ cm^{-3} to about 50 μs at $\Delta n \sim 10^{10}$ cm^{-3}. A similar low-injection recombination is observed for SiN$_x$-passivated p-type surfaces,[64] which exhibit a surface depletion region (SDR) due to the fixed positive
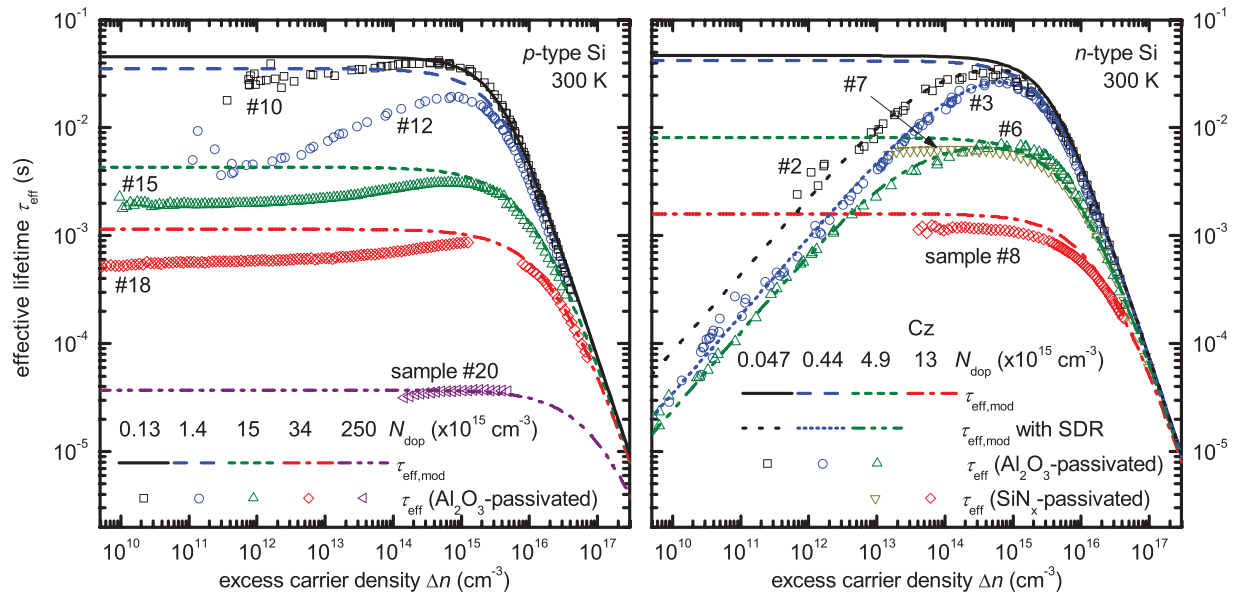

FIG. 4. (Color online) Effective lifetime for p-type (left) and n-type (right) Si wafers with various bulk resistivities measured at 300 K (with sample number according to Table I). The samples were passivated either with Al$_2$O$_3$ or SiN$_x$. The lines represent the modeled effective lifetime $\tau_{\text{eff,mod}}$ according to Eq. (14), which includes $\tau_{\text{intr,adv}}$ and τ_{extr}. For the Al$_2$O$_3$-passivated n-type samples, additional lines indicate a more complete modeling that also includes recombination in the surface depletion region (SDR) according to Eq. (16).
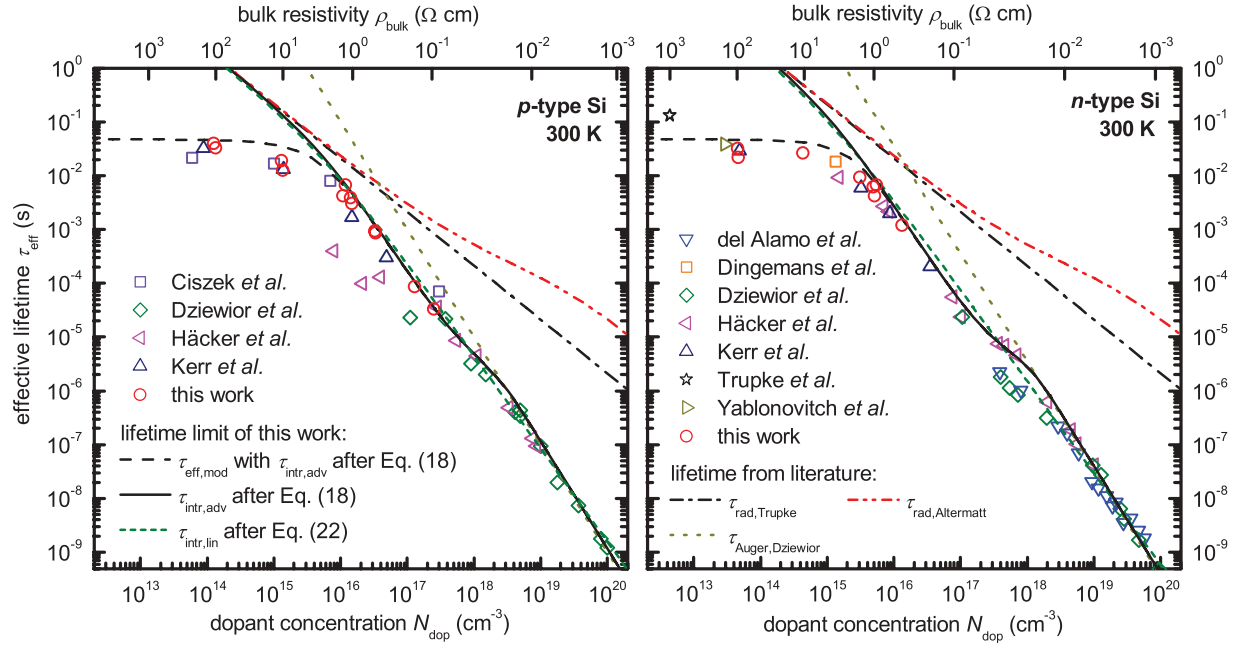
FIG. 5. (Color online) Maximum effective lifetime as a function of the dopant concentration measured at 300 K on *p*-type (left) and *n*-type (right) silicon, together with literature data (Refs. 10,48,52,71–75). The data are compared to the effective lifetime limit $\tau_{\text{eff,mod}}$ after Eq. (14) including $\tau_{\text{intr,adv}}$ and the assumed τ_{extr}. Also plotted are the intrinsic lifetime limit of this work, $\tau_{\text{intr,adv}}$ of Eq. (18), and the simpler Eq. (22), $\tau_{\text{intr,lin}}$. In addition, τ_{rad} according to Trupke *et al.* (Ref. 30), and according to Altermatt *et al.* (Ref. 49), as well as the free-particle Auger lifetime with the Auger coefficients after Dziewior and Schmid, Eqs. (2) and (3) are also given.

charge of SiN$_x$ layers.[65] The Al$_2$O$_3$/Si interface is known to feature a high fixed negative charge;[66–69] thus a SDR is formed on *n*-type surfaces due to the repulsion of electrons from the Al$_2$O$_3$/Si interface. Recombination within such SDRs is believed to be the origin of the strong injection-dependent effective lifetime in low injection.[65,70] Thus, for the Al$_2$O$_3$-passivated *n*-type samples, the decreasing lifetime in low injection can be attributed to surface effects, but not to silicon bulk defects. Consistent with this SDR argument, the SiN$_x$-passivated *n*-type samples do not show a decreasing lifetime in low injection.

In Fig. 5 the maximum measured effective lifetime of all *p*-type and *n*-type samples is compared to literature data as a function of the dopant concentration. For $N_{\text{dop}} > 5 \times 10^{15}$ cm^{-3}, all of the data form two straight-line regions: the CE-AR region for $N_{\text{dop}} < 10^{17}$ cm^{-3}, and the traditional free-particle Auger recombination region for $N_{\text{dop}} > 5 \times 10^{18}$ cm^{-3}, with the Mott transition region in between. For $N_{\text{dop}} < 5 \times 10^{15}$ cm^{-3}, however, the measured lifetime data stay significantly below the CE-AR straight-line region, which cannot be explained by intrinsic recombination processes. This deviation is typically attributed to SRH recombination,[5,6] and thus, the maximum measured effective lifetime of the samples with $N_{\text{dop}} < 2 \times 10^{15}$ cm^{-3} is either dominated by surface or bulk recombination or a combination of both, but not by radiative or Auger recombination.

The preceding discussion stresses the fact that, despite technological advances, it is almost impossible in practice to completely suppress SRH recombination, either at very low majority carrier concentrations (i.e., dopant densities) or very low minority carrier concentrations. Such conditions are not conducive to strong Auger or band-to-band recombination,

and it is not surprising that extrinsic processes, either in the bulk or at the surfaces, become predominant. We focus next on the extraction of the Auger recombination rate in the range where it is clearly dominant.

IV. EXTRACTION OF THE AUGER RECOMBINATION RATE FROM MEASURED LIFETIME DATA

A. Modeling of lifetime data

In order to quantitatively extract Auger recombination from the measured effective lifetime data, we modeled the latter as the reciprocal sum of the lifetimes related to the different recombination mechanisms:

$$\frac{1}{\tau_{\text{eff}}} = \frac{1}{\tau_{\text{rad}}} + \frac{1}{\tau_{\text{Auger}}} + \frac{1}{\tau_{\text{bulk,SRH}}} + \frac{1}{\tau_{\text{surf}}}, \quad (12)$$

where τ_{rad} is the lifetime associated with the radiative recombination, τ_{Auger} the Auger lifetime, $\tau_{\text{bulk,SRH}}$ the SRH lifetime of the bulk defect recombination, and τ_{surf} the surface recombination related lifetime. As the contribution of $\tau_{\text{bulk,SRH}}$ and τ_{surf} cannot be distinguished unambiguously for most of our measured lifetime data, we define an effective extrinsic recombination lifetime τ_{extr} which accounts for both:

$$\frac{1}{\tau_{\text{extr}}} \equiv \frac{1}{\tau_{\text{SRH,bulk}}} + \frac{1}{\tau_{\text{surf}}}. \quad (13)$$

Thus, the modeled effective lifetime can be written as

$$\frac{1}{\tau_{\text{eff,mod}}} = \frac{1}{\tau_{\text{intr}}} + \frac{1}{\tau_{\text{extr}}}, \quad (14)$$
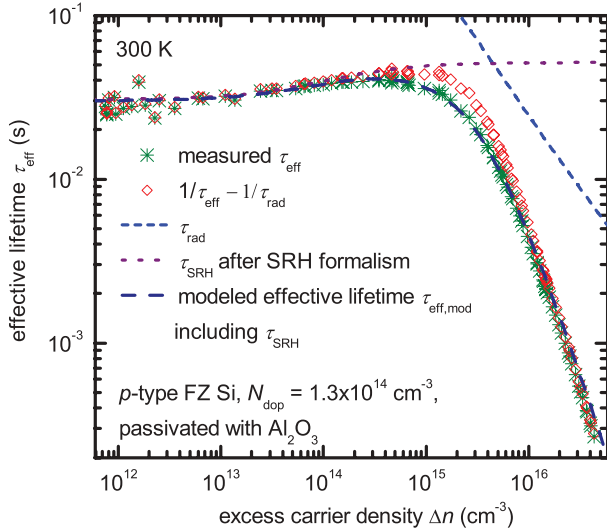
FIG. 6. (Color online) Measured τ_{eff} for the Al_2O_3-passivated p-type FZ Si sample with $N_{\text{dop}} = 1.3 \times 10^{14}$ cm^{-3} (sample #10) compared to the lifetime resulting from the reciprocal subtraction of τ_{rad}. Additionally, the modeled effective lifetime $\tau_{\text{eff,mod}}$ for this sample according to Eq. (14) is shown too, where $\tau_{\text{intr,adv}}$ was used for the intrinsic lifetime limit and the extrinsic lifetime was modeled according to the SRH formalism with a single defect level.

with the intrinsic lifetime

$$\frac{1}{\tau_{\text{intr}}} = \frac{1}{\tau_{\text{rad}}} + \frac{1}{\tau_{\text{Auger}}}. \qquad (15)$$

The radiative recombination can be modeled with the radiative recombination coefficient measured by Trupke *et al.* for lowly doped silicon B_{low} which has a value of 4.73×10^{-15} cm^3/s at 300 K.[30] We also account for the Coulomb-enhanced radiative recombination model proposed by Altermatt *et al.*[31] according to the parametrization of the relative radiative recombination coefficient $B_{\text{rel}}(n_0, p_0, \Delta n)$ given in Ref. 49. The radiative recombination coefficient B is then the product of B_{low} and B_{rel}.

To extract the Auger recombination we assume a constant value of the effective extrinsic SRH recombination,[76] independent of N_{dop} and Δn. In order to estimate such a value, we subtract $1/\tau_{\text{rad}}$ from the measured effective lifetime of the sample with the highest lifetime, which is the Al_2O_3-passivated p-type sample with $N_{\text{dop}} = 1.3 \times 10^{14}$ cm^{-3}. This is shown in Fig. 6. The effective lifetime corrected for the radiative recombination shows a maximum value of $\sim$47 ms, and thus we used $\tau_{\text{extr}} = 47$ ms. This value was found to model our maximum measured lifetime data adequately. Trupke *et al.* reported a measured effective lifetime of 130 ms for n-type silicon wafer with $N_{\text{dop}} = 4.3 \times 10^{12}$ cm^{-3},[48] which indicates that high-quality ultra-lowly-doped silicon may present even higher lifetimes than we have observed and that τ_{extr} might be a function of the dopant concentration for this ultra-lowly-doped silicon. To verify this, however, more experimental data for such material is necessary, and therefore we decided to use a more conservative value.

As the measured lifetime of the Al_2O_3-passivated n-type samples is dominated by SDR recombination in low injection,

we additionally took a term for SDR recombination into account. There are different approaches to model the SDR recombination.[18,70,77] We applied the model according to Refs. 18 and 77, which explains the measured low-injection lifetime of all our Al_2O_3-passivated n-type samples very well. This model describes the SDR recombination by means of a recombination current density prefactor J_0 in combination with an ideality factor m, as typically used for the recombination within a space-charge region. Accordingly, the lifetime related to SDR recombination can be expressed as

$$\frac{1}{\tau_{\text{SDR}}} = \frac{2}{W} \frac{J_0}{e \Delta n} \left[\left(\frac{\Delta n}{n_{0,\text{min}}} + 1 \right)^{1/m} - 1 \right], \qquad (16)$$

where e is the elementary charge, and $n_{0,\text{min}}$ the thermal equilibrium minority carrier density. To determine values for J_0 and m, τ_{SDR} was fitted to the measured low-injection lifetime for each Al_2O_3-passivated n-type sample separately, treating J_0 and m as fitting parameters. The determined values are given in Table I. It is worth mentioning that a subtraction of this SDR lifetime from the τ_{rad} corrected effective lifetime of sample #2 (n-type sample with $N_{\text{dop}} = 4.6 \times 10^{13}$ cm^{-3}) analogous to that shown in Fig. 6 for the p-type sample with $N_{\text{dop}} = 1.3 \times 10^{14}$ cm^{-3}, results in the same maximum lifetime level around 47 ms. Therefore, a value for τ_{extr} of 47 ms applies to both the p-type and n-type samples.

To calculate $n_{0,\text{min}}$ from the thermal equilibrium majority carrier density we applied the effective intrinsic carrier concentration $n_{\text{i,eff}}$ which is given by following relation:[78]

$$n_{\text{i,eff}} = n_i e^{\beta \Delta E_g / 2}, \qquad (17)$$

where n_i is the intrinsic carrier concentration, ΔE_g the energy band-gap narrowing, and $\beta = 1/k_B T$, with the Boltzmann constant k_B and the absolute temperature T. We used a n_i value measured by Misiakos and Tsamakis, which is 9.7×10^9 cm^{-3} at 300 K.[79] As Altermatt *et al.* pointed out, this value is in good agreement with older measurements.[78] This n_i value is also consistent with the determination of B_{low} by Trupke *et al.*,[30] as they also used the values of Misiakos and Tsamakis. To account for band-gap narrowing, we calculate ΔE_g according to the random-phase approximation model proposed by Schenk.[80] This calculation of $n_{\text{i,eff}}$ was used throughout this work.

B. Quantitative description of Auger recombination

Based on our effective lifetime measurements for lowly and moderately doped silicon, together with literature data for highly doped silicon,[10,72,74] it is possible to describe the Auger recombination rate in a general manner as a function of the dopant concentration and the excess carrier density for crystalline silicon at 300 K, using an expression similar to that of Kerr and Cuevas.[21] As a difference with respect to that previous study, and to account for Coulomb-enhanced Auger recombination according to the theory of Hangleiter and Häcker,[12] we have applied enhancement factors g_{eeh} and g_{ehh} similar to the empirical parametrizations of Eqs. (4) and (5) as introduced by Altermatt *et al.*[6] We further included the radiative recombination in our expression with the product $B_{\text{rel}} B_{\text{low}}$, as this was used to extract the Auger recombination

TABLE II. Advanced parametrization for the intrinsic lifetime $\tau_{\mathrm{intr,adv}}$ of crystalline silicon at 300 K including the improved parametrization of Coulomb-enhanced Auger recombination. All parameters are specified in Table III.

$$\tau_{\mathrm{intr,adv}} = \frac{\Delta n}{\left(np - n_{\mathrm{i,eff}}^2\right)\left(2.5 \times 10^{-31} g_{\mathrm{eeh}} n_0 + 8.5 \times 10^{-32} g_{\mathrm{ehh}} p_0 + 3.0 \times 10^{-29} \Delta n^{0.92} + B_{\mathrm{rel}} B_{\mathrm{low}}\right)} \tag{18}$$

with the enhancement factors

$$g_{\mathrm{eeh}}(n_0) = 1 + 13\left\{1 - \tanh\left[\left(\frac{n_0}{N_{0,\mathrm{eeh}}}\right)^{0.66}\right]\right\} \text{ and } g_{\mathrm{ehh}}(p_0) = 1 + 7.5\left\{1 - \tanh\left[\left(\frac{p_0}{N_{0,\mathrm{ehh}}}\right)^{0.63}\right]\right\}, \tag{19}$$

and $N_{0,\mathrm{eeh}} = 3.3 \times 10^{17}$ cm^{-3} and $N_{0,\mathrm{ehh}} = 7.0 \times 10^{17}$ cm^{-3}.

from the measurements. Therefore, the resulting parametrization describes all *intrinsic* recombination in silicon. It can be expressed as a recombination lifetime of the minority carriers $\tau_{\mathrm{intr,adv}}$ given by Eq. (18) of Table II, with all the parameters specified in Table III. Possible simplifications to $\tau_{\mathrm{intr,adv}}$, in particular concerning $n_{\mathrm{i,eff}}$ and B_{rel}, are discussed in the Appendix together with their respective ranges of applicability.

It should be pointed out that this parametrization is not significantly affected by the assumed τ_{extr} of 47 ms. In the high-injection regime it is exclusively based on the lifetime data above $\Delta n \sim 5 \times 10^{15}$ cm^{-3}, which is clearly dominated by Auger recombination. Concerning the low-injection regime, it is important to note that the low-injection lifetime of the samples with N_{dop} around 5×10^{15} cm^{-3} and above is predominantly limited by Auger recombination, while for N_{dop} of 1×10^{15} cm^{-3} and below it is dominated by τ_{extr} (cf. Fig. 5 and Sec. III B). Therefore, the parametrization of the low-injection Auger recombination was based only on the measured low-injection lifetime of the samples with $N_{\mathrm{dop}} \geqslant 5 \times 10^{15}$ cm^{-3}. Hence, the low-injection Auger parametrization is not significantly affected by the assumed τ_{extr} either. To illustrate the applicability of the parametrization, Fig. 6 compares the modeled and measured effective lifetimes for sample #10, where the extrinsic recombination was modeled according to the SRH formalism with a single defect level,[81] and not with $\tau_{\mathrm{extr}} = 47$ ms. As can be seen, both are in excellent agreement over the whole carrier injection range. A similar agreement between model and experiment has been observed for all *p*-type samples that show a decreasing and saturating lifetime in low injection, the typical shape of SRH recombination. This indicates that the improved quantitative description of Auger recombination, together with the SRH formalism is able to describe the experimental evidence, and

further justifies the assumption of the constant τ_{extr} to extract a unique Auger parametrization.

The lower graphs of Fig. 7 show the relative deviation of the improved parametrization for the intrinsic lifetime with respect to the measured effective lifetime $\tau_{\mathrm{intr,adv}}/\tau_{\mathrm{eff}}$ for all *p*-type (left) and *n*-type (right) samples. With this notation, an underestimation leads to values $\tau_{\mathrm{intr,adv}}/\tau_{\mathrm{eff}} < 1$. The 20% uncertainty range of our measured effective lifetime is also plotted in the graphs (gray dashed lines). It can be seen that for Δn above $\sim 5 \times 10^{15}$ cm^{-3}, the high-injection Auger-dominated region, almost all deviations are constant at a certain level within our uncertainty range, indicating that the high-injection slope of our parametrization predicts very well the slope of the measured high-injection lifetime data. In contrast, the same deviations for $\tau_{\mathrm{intr,Kerr}}$ plotted in the upper graphs show a considerable positive slope leading to a significant overestimation of the intrinsic recombination. For the samples with N_{dop} below $\sim 2 \times 10^{15}$ cm^{-3}, $\tau_{\mathrm{intr,adv}}/\tau_{\mathrm{eff}}$ is considerably above 1 for Δn below $\sim 5 \times 10^{15}$ cm^{-3} indicating a significant overestimation of τ_{eff}. However, as the low-injection lifetime of these samples is not limited by intrinsic recombination as quantified with $\tau_{\mathrm{intr,adv}}$ but by defect recombination, such an overestimation can be expected, even for Δn around 10^{15} cm^{-3}.

Figure 4 compares the measured effective lifetime data of the *p*-type and *n*-type silicon samples with the modeled effective lifetime $\tau_{\mathrm{eff,mod}}$ according to Eq. (14) using $\tau_{\mathrm{intr,adv}}$ given by Eq. (18) as intrinsic lifetime limit. It can be seen that $\tau_{\mathrm{eff,mod}}$ is in very good agreement with the measured data for *p*-type and *n*-type silicon, in particular at high injection. The low-injection lifetime of the *p*-type samples is slightly overestimated, due to the rather simple approximation of τ_{extr} with an injection-independent constant value. As mentioned above, an even better fit can be obtained by adding the defect SRH

TABLE III. Parameters of Eq. (18).

Parameter	Unit	Description
n	cm^{-3}	Electron density
p	cm^{-3}	Hole density
n_0	cm^{-3}	Thermal equilibrium electron density
p_0	cm^{-3}	Thermal equilibrium hole density
Δn	cm^{-3}	Excess carrier density
n_{i}	cm^{-3}	Intrinsic carrier concentration for lowly doped and lowly injected silicon, 9.7×10^9 cm^{-3} at 300 K (Ref. 79)
$n_{\mathrm{i,eff}}$	cm^{-3}	Effective intrinsic carrier concentration, according to Eq. (17)
B_{low}	cm^{-3} s^{-1}	Radiative recombination coefficient for lowly doped and lowly injected silicon, 4.73×10^{-15} cm^3 s^{-1} at 300 K (Ref. 30)
B_{rel}	–	Relative radiative recombination coefficient, according to Ref. 49
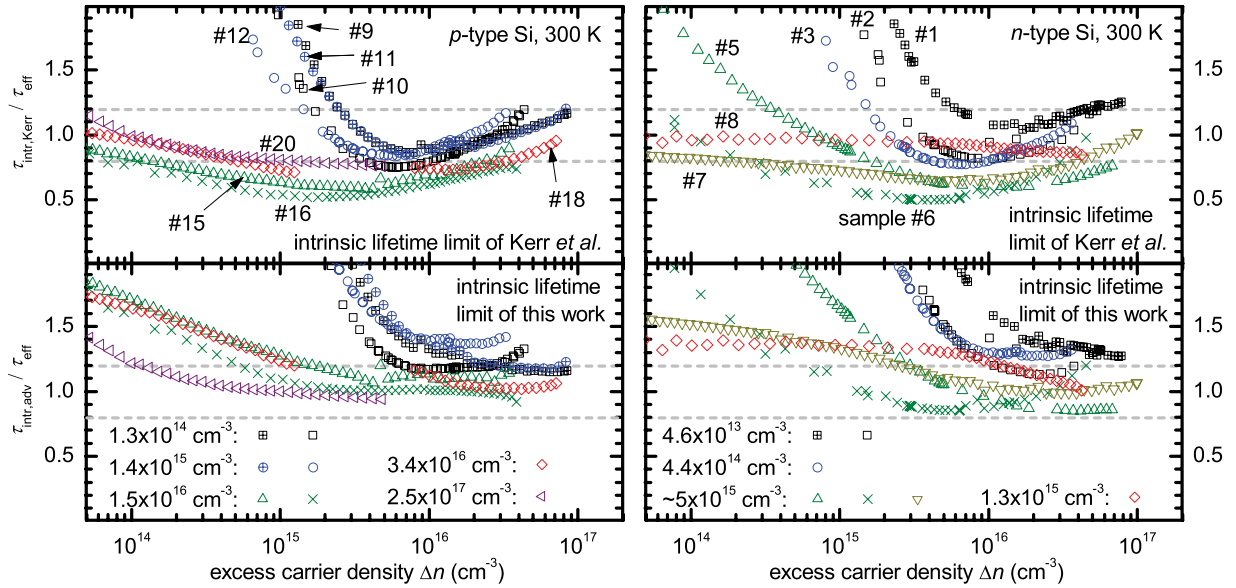
FIG. 7. (Color online) Relative deviation $\tau_{\mathrm{intr}}/\tau_{\mathrm{eff}}$ of the intrinsic lifetime limit τ_{intr} and the measured effective lifetime τ_{eff} for the p-type (left) and the n-type (right) samples. The upper graphs show the relative deviation for Kerr's parametrization, Eq. (6), the lower graphs for the advanced parametrization of this work, Eq. (18). The samples are labeled according to Table I. The gray lines mark the relative uncertainty range of 20% of our lifetime measurements, obtained from the lifetime measurement comparison in Sec. III C.

contribution. It is worth mentioning that the SDR recombination according to Eq. (16) predicts the measured low-injection lifetime of the Al_2O_3-passivated n-type samples very well.

V. DISCUSSION

To be consistent with the Coulomb-enhanced Auger recombination (CE-AR) theory of Hangleiter and Häcker, we have applied in our quantitative description of the Auger recombination of Eq. (18) enhancement factors g_{eeh} and g_{ehh} analogous to those introduced by Altermatt *et al.*[6] These enhancement factors describe very well the characteristic CE-AR hump of the experimentally determined Auger-dominated low-injection lifetime for $N_{\mathrm{dop}} > 5 \times 10^{15}$ cm^{-3} with a transition region around 1×10^{18} cm^{-3} (cf. Fig. 5). If CE-AR behaved symmetrically in N_{dop} and Δn, one would expect to observe a similar hump *also* for lowly doped silicon under high injection, with a similar transition region starting at Δn around 10^{17} cm^{-3}, as suggested by Schmidt *et al.*[20] However, such a transition region and the related shape are not exhibited by the measured lifetime data in high injection (cf. Fig. 4), nor have they been reported in the literature. For example, the effective lifetime, corrected by radiative recombination, of the p-type sample with $N_{\mathrm{dop}} = 1.3 \times 10^{14}$ cm^{-3} shown in Fig. 6, presents a straight-line behavior in the Auger-dominated high-injection range. It is possible that the CE-AR characteristic hump is not visible due to the fact that our lifetime measurements are limited to a maximum injection level of about 5×10^{16} cm^{-3}. Nevertheless, Hangleiter and Häcker mentioned in their work on CE-AR of lowly injected silicon that under high excitation of lowly doped silicon a stronger shielding is expected than for low excitation of highly doped silicon, due to the equal densities of electrons and holes.[12] Thus, the transition region would be shifted to even lower Δn values, towards the range we have measured. As the

physical nature of the CE-AR mechanism in high injection is not completely understood yet, and since we have not observed the CE-AR characteristic hump under high injection, we have included in our parametrization enhancement factors only for the thermal equilibrium carrier densities, n_0 and p_0.

In Fig. 8, these enhancement factors are compared to the theoretically determined values of Hangleiter and Häcker[12] exemplarily for n-type silicon, i.e., for g_{eeh}. For high carrier concentrations above 1×10^{18} cm^{-3}, the theoretically determined g_{eeh} overestimates the experimentally determined g_{eeh} of Altermatt *et al.* and of this work considerably. The same holds also for g_{ehh} of p-type silicon, and was
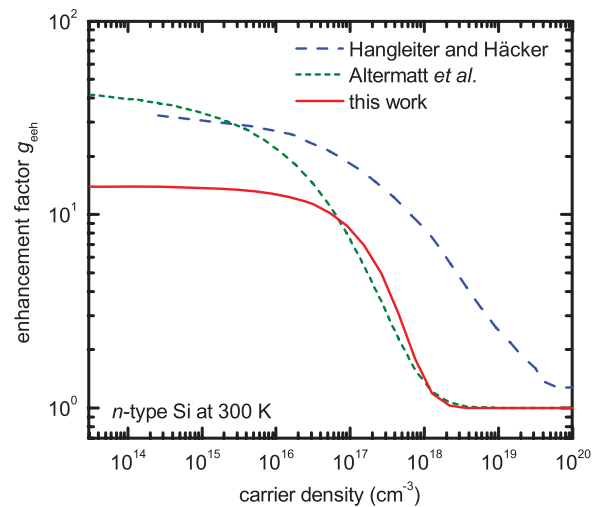
FIG. 8. (Color online) Enhancement factor g_{eeh} for lowly injected n-type silicon. The experimentally quantified g_{eeh} of Altermatt *et al.*, Eq. (4), and this work, Eq. (19), are compared to the theoretically determined g_{eeh} of Hangleiter and Häcker (Ref. [12]).

observed by Häcker and Hangleiter for g_{eeh} and g_{ehh} also.[74] Due to some scattering of the experimentally determined low-injection lifetime in the range of the transition region around 5×10^{17} cm^{-3}, there is small uncertainty of the experimentally determined enhancement factors in this range. However, for low carrier concentrations below 10^{16} cm^{-3}, where the theoretically determined g_{eeh} is in good agreement with the g_{eeh} of Altermatt *et al.*, the g_{eeh} extracted from our experimental data is more than a factor of 2 lower than the theoretically determined g_{eeh}. Again, the same trend even more pronounced is observed for g_{ehh} also. This indicates that the quantum-mechanical theory of Hangleiter and Häcker for lowly injected silicon overestimates the Coulomb enhancement of the Auger recombination (due to the formation of excitons) not only for high carrier concentrations, but also for low carrier concentrations. One possible explanation can be the scattering of mobile charge carriers at locally fixed ionized dopant atoms. This was not accounted for in the CE-AR theory of Hangleiter and Häcker, but was found to be important for modeling other physical mechanisms, in particular the charge carrier mobility in silicon.[43]

VI. SUMMARY

The recent advances in surface passivation techniques for silicon wafers, in particular for depositing Al_2O_3 and SiN_x, have permitted the study of silicon bulk recombination more precisely than ever before. In this work we have measured the injection-dependent effective lifetime of high-purity silicon wafers as a function of the dopant concentration (phosphorus or boron) by applying such surface passivation layers. We found that in many cases the measured effective lifetime exceeds the previously accepted values for the intrinsic recombination proposed by Kerr and Cuevas.[21] To assess the accuracy of our lifetime measurements we have compared two different measurement techniques at two different laboratories, from which we determined a relative uncertainty of $\pm 20\%$. In comparison, the discrepancy between the measured lifetime and Kerr's expression for the intrinsic lifetime was found to be as high as 50% for lowly doped silicon at medium injection levels. To quantify Auger recombination based on our experimental lifetime results, we have developed a parametrization for the intrinsic lifetime of n-type and p-type crystalline silicon at 300 K, which is consistent with the theory of Coulomb-enhanced Auger recombination (CE-AR) and accounts for Coulomb-enhanced radiative recombination. This parametrization provides excellent accuracy to describe the upper limit of the minority carrier lifetime in crystalline silicon for a wide range of dopant densities, as well as a broad range of carrier injection levels. A comparison with the results of CE-AR theory for lowly injected silicon of Hangleiter and Häcker[12] revealed that the theory considerably underestimates the low-injection Auger lifetime not only for high carrier concentrations, but also for low carrier concentrations.
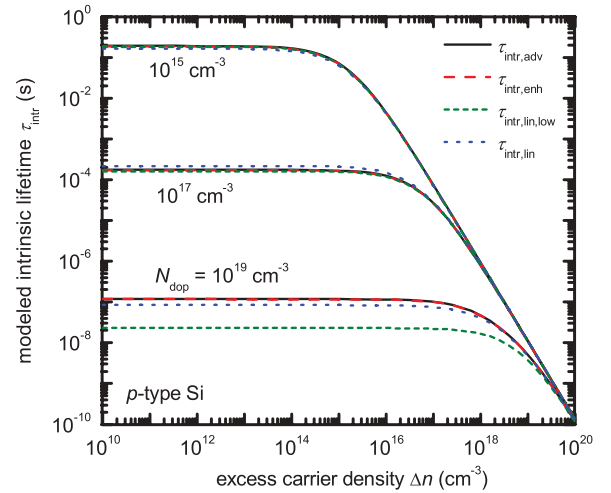
ACKNOWLEDGMENTS

FIG. 9. (Color online) Intrinsic lifetime calculated with the parametrizations given in Eqs. (20)–(22) compared to the full parametrization of Eq. (18) for p-type Si.

APPENDIX: SIMPLIFIED EXPRESSIONS FOR THE INTRINSIC LIFETIME LIMIT

The parametrization of the intrinsic lifetime derived in this work given in Eq. (18) contains $n_{i,eff}$ and B_{rel}, which were calculated according to rather complex state-of-the-art models. Therefore, in this section we discuss some simplifications to improve the practical application of the parametrization.

In the term $(np - n_{i,eff}^2)$ of Eq. (18), $n_{i,eff}^2$ accounts for the thermal recombination in the thermal equilibrium in dark. For $\Delta n \gg n_{i,eff}$ and $N_{dop} \gg n_{i,eff}$, this term can be
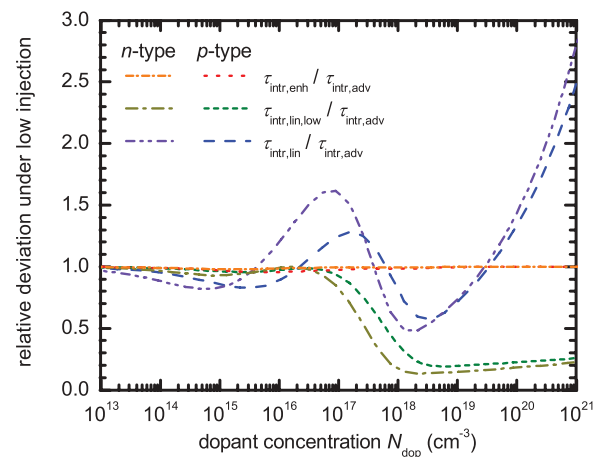

FIG. 10. (Color online) Relative deviation of the modeled intrinsic low-injection lifetime of Eqs. (20)–(22) with respect to the full parametrization of Eq. (18) for n-type and p-type Si.

TABLE IV. Simplified equations for the intrinsic lifetime parametrization of this work $\tau_{\mathrm{intr,adv}}$ given in Eq. (18): Equation (20) without $n_{\mathrm{i,eff}}$ and B_{rel} and Eq. (21) additionally without the enhancement factors g_{eeh} and g_{ehh}, which fits the Eq. (18) for low dopant concentrations. Equation (22) presents a polynomial parametrization without enhancement factors for the whole N_{dop} range. The maximum relative deviation from $\tau_{\mathrm{intr,adv}}$ is also quoted. All parameters are specified in Table III.

Simplified model for the intrinsic lifetime with enhancement factors and *without* $n_{\mathrm{i,eff}}$ and B_{rel}:

$$\tau_{\mathrm{intr,enh}} = \frac{\Delta n}{np(2.5 \times 10^{-31} g_{\mathrm{eeh}} n_0 + 8.5 \times 10^{-32} g_{\mathrm{ehh}} p_0 + 3.0 \times 10^{-29} \Delta n^{0.92} + B_{\mathrm{low}})}, \qquad (20)$$

with the enhancement factors according to Eq. (19); maximum relative deviation $\max_{\Delta n, N_{\mathrm{dop}}} |1 - \tau_{\mathrm{intr,enh}}/\tau_{\mathrm{intr,adv}}| < 4\%$.

Linear model for the intrinsic lifetime *without* enhancement factors, which fits Eq. (18) for low dopant concentrations:

$$\tau_{\mathrm{intr,lin,low}} = \frac{\Delta n}{np(8.7 \times 10^{-29} n_0^{0.91} + 6.0 \times 10^{-30} p_0^{0.94} + 3.0 \times 10^{-29} \Delta n^{0.92} + B_{\mathrm{low}})}; \qquad (21)$$

Maximum relative deviation $\max_{\Delta n, N_{\mathrm{dop}}} |1 - \tau_{\mathrm{intr,lin,low}}/\tau_{\mathrm{intr,adv}}| < 10\%$ for $N_{\mathrm{dop}} < 6 \times 10^{16}$ cm^{-3}.

Linear model for the intrinsic lifetime *without* enhancement factors for the whole N_{dop} range (less accurate than Eq. (21) for $N_{\mathrm{dop}} < 6 \times 10^{16}$ cm^{-3}):

$$\tau_{\mathrm{intr,lin}} = \frac{\Delta n}{np(1.1 \times 10^{-25} n_0^{0.71} + 1.6 \times 10^{-26} p_0^{0.73} + 3.0 \times 10^{-29} \Delta n^{0.92} + B_{\mathrm{low}})}; \qquad (22)$$

maximum relative deviation $\max_{\Delta n, N_{\mathrm{dop}}} |1 - \tau_{\mathrm{intr,lin}}/\tau_{\mathrm{intr,adv}}| < 60\%$ for $N_{\mathrm{dop}} < 10^{20}$ cm^{-3}.

---

approximated by np. Additionally, $n_{\mathrm{i,eff}}$ is used to calculate the thermal equilibrium minority carrier density from the thermal equilibrium majority carrier density. For $N_{\mathrm{dop}} \gg n_{\mathrm{i,eff}}$, however, the contribution of the thermal equilibrium minority carriers can be neglected as the thermal equilibrium majority carrier density is more than three orders of magnitude higher.

The contribution of B_{rel} on τ_{rad} can be seen in Fig. 5 as a function of N_{dop}. Compared are $\tau_{\mathrm{rad,Altermatt}}$, which was calculated with the product $B_{\mathrm{rel}} B_{\mathrm{low}}$, and $\tau_{\mathrm{rad,Trupke}}$, which was calculated only with B_{low}. For N_{dop} above $\sim 10^{17}$ cm^{-3}, $\tau_{\mathrm{rad,Altermatt}}$ begins to differ from $\tau_{\mathrm{rad,Trupke}}$. In this range, however, Auger recombination clearly dominates and thus, B_{rel} as a function of N_{dop} is negligible. The same argumentation also holds for B_{rel} as a function of Δn.

Therefore, we introduce with $\tau_{\mathrm{intr,enh}}$, [Eq. (20) in Table IV], a parametrization with the following simplifications to the full parametrization of Eq. (18): (i) neglecting the term $n_{\mathrm{i,eff}}^2$, and thus the thermal equilibrium recombination, (ii) neglecting the thermal equilibrium minority carrier concentration, and (iii) assuming $B_{\mathrm{rel}} = 1$, thus not accounting for the Coulomb-enhanced radiative recombination. In Fig. 9 $\tau_{\mathrm{intr,enh}}$ is compared to $\tau_{\mathrm{intr,adv}}$ as a function of Δn for three different dopant concentrations of *p*-type silicon. It can be seen that for a Δn range from 10^{10} to 10^{20} cm^{-3} and for a N_{dop} range from 10^{15} to 10^{19} cm^{-3} both parametrizations are in very good agreement. The relative deviation $\tau_{\mathrm{intr,enh}}/\tau_{\mathrm{intr,adv}}$ is less than 4%, which holds also for even smaller N_{dop} values and in particular, also for *n*-type silicon. This can also be seen from

the relative deviation $\tau_{\mathrm{intr,enh}}/\tau_{\mathrm{intr,adv}}$ in low injection shown in Fig. 10 as a function of N_{dop}. Thus, $\tau_{\mathrm{intr,enh}}$ is a reasonable simplification of $\tau_{\mathrm{intr,adv}}$.

Following the approach of Kerr and Cuevas without enhancement factors, a simple fit to the measured effective lifetime data is given by $\tau_{\mathrm{intr,lin}}$ according to [Eq. (22) in Table IV]. In Fig. 5 the low-injection lifetime of $\tau_{\mathrm{intr,lin}}$ is compared to the low-injection lifetime of $\tau_{\mathrm{intr,adv}}$ as well as to measured effective lifetime data. As can be seen, $\tau_{\mathrm{intr,lin}}$ features a *linear* shape in the CE-AR transition region around $N_{\mathrm{dop}} = 10^{18}$ cm^{-3}. This leads to an overestimation of the measured lifetime data directly above the transition region and to an underestimation directly below, although measured lifetime data are rare in this range, in particular around $N_{\mathrm{dop}} = 10^{17}$ cm^{-3}. As can be seen, around the transition region $\tau_{\mathrm{intr,adv}}$ gives a better fit to maximum measured lifetime values. Figure 10 shows the relative deviation of $\tau_{\mathrm{intr,lin}}$ and $\tau_{\mathrm{intr,adv}}$, which is $\sim 60\%$ ($\sim 50\%$) for *n*-type Si and $\sim 30\%$ ($\sim 40\%$) for *p*-type Si above (below) the CE-AR transition region. For $N_{\mathrm{dop}} > 5 \times 10^{19}$ cm^{-3} the deviation increases significantly as $\tau_{\mathrm{intr,lin}}$ does not converge to the free-particle Auger lifetime for high dopant concentrations according to Eqs. (2) and (3), even if there is only limited lifetime data available in this range. The linear fit of $\tau_{\mathrm{intr,lin}}$ can be improved by restricting it to dopant concentrations below 6×10^{16} cm^{-3}. Such a fit is given by $\tau_{\mathrm{intr,lin,low}}$ according to [Eq. (21) in Table IV]. As can be seen from Figs. 9 and 10 $\tau_{\mathrm{intr,lin,low}}$ is in good agreement with $\tau_{\mathrm{intr,adv}}$ for $N_{\mathrm{dop}} < 6 \times 10^{16}$ cm^{-3}, indicated by a deviation of less than 10%.

---

[*]Corresponding author: armin.richter@ise.fraunhofer.de

[1]M. S. Tyagi and R. van Overstraeten, Solid-State Electron. **26**, 577 (1983).

[2]S. M. Sze and K. K. Ng, *Physics of Semiconductor Devices*, 3rd ed. (John Wiley & Sons, Hoboken, NJ, 2007).

[3]M. A. Green, IEEE Trans. Electron Devices **31**, 671 (1984).

[4]T. Tiedje, E. Yablonovitch, G. D. Cody, and B. G. Brooks, IEEE Trans. Electron Devices **31**, 711 (1984).

[5]E. Yablonovitch and T. Gmitter, Appl. Phys. Lett. **49**, 587 (1986).

[6]P. P. Altermatt, J. Schmidt, G. Heiser, and A. G. Aberle, J. Appl. Phys. **82**, 4938 (1997).

[7]A. R. Beattie and P. T. Landsberg, Proc. R. Soc. London A **249**, 16 (1959).

[8]A. Haug, Solid State Electron. **21**, 1281 (1978).

[9]L. Huldt, Phys. Status Solidi A **8**, 173 (1971).

[10]J. Dziewior and W. Schmid, Appl. Phys. Lett. **31**, 346 (1977).

[11]R. A. Sinton and R. M. Swanson, IEEE Trans. Electron Devices **34**, 1380 (1987).

[12]A. Hangleiter and R. Häcker, Phys. Rev. Lett. **65**, 215 (1990).

[13]D. B. Laks, G. F. Neumark, and S. T. Pantelides, Phys. Rev. B **42**, 5176 (1990).

[14]M. Govoni, I. Marri, and S. Ossicini, Phys. Rev. B **84**, 075215 (2011).

[15]P. T. Landsberg, Appl. Phys. Lett. **50**, 745 (1987).

[16]The coefficient of the radiative recombination B can be determined directly, i.e., by the spontaneous emission of the radiative recombination processes (Ref. 22), or from the absorption spectrum of its inverse effect, the band-to-band transition under illumination (Ref. 30).

[17]D. A. Clugston and P. A. Basore, in *Proceedings of the 26th IEEE Photovoltaic Specialists Conference, Anaheim, CA* (IEEE, New York, USA, 1997), p. 207.

[18]S. W. Glunz, D. Biro, S. Rein, and W. Warta, J. Appl. Phys. **86**, 683 (1999).

[19]P. P. Altermatt, J. Schmidt, M. Kerr, G. Heiser, and A. G. Aberle, in *Proceedings of the 16th European Photovoltaic Solar Energy Conference, Glasgow, UK* (James & James, London, UK, 2000), p. 243.

[20]J. Schmidt, M. Kerr, and P. P. Altermatt, J. Appl. Phys. **88**, 1494 (2000).

[21]M. J. Kerr and A. Cuevas, J. Appl. Phys. **91**, 2473 (2002).

[22]H. Schlangenotto, H. Maeder, and W. Gerlach, Phys. Status Solidi A **21**, 357 (1974).

[23]G. Agostinelli, A. Delabie, P. Vitanov, Z. Alexieva, H. F. W. Dekkers, S. De Wolf, and G. Beaucarne, Sol. Energy Mater. Sol. Cells **90**, 3438 (2006).

[24]B. Hoex, S. B. S. Heil, E. Langereis, M. C. M. van de Sanden, and W. M. M. Kessels, Appl. Phys. Lett. **89**, 042112 (2006).

[25]J. Benick, A. Richter, M. Hermle, and S. W. Glunz, Phys. Status Solidi RRL **3**, 233 (2009).

[26]J. Schmidt, B. Veith, and R. Brendel, Phys. Status Solidi RRL **3**, 287 (2009).

[27]G. Dingemans, M. C. M. van de Sanden, and W. M. M. Kessels, Electrochem. Solid-State Lett. **13**, H76 (2010).

[28]D. Suwito, T. Roth, D. Pysch, L. Korte, A. Richter, S. Janz, and S. W. Glunz, in *Proceedings of the 23rd European Photovoltaic Solar Energy Conference, Valencia, Spain* (WIP, Munich, Germany, 2008), p. 1023.

[29]T. Lüder, G. Hahn, and B. Terheiden, Energy Procedia **8**, 660 (2011).

[30]T. Trupke, M. A. Green, P. Würfel, P. P. Altermatt, A. Wang, J. Zhao, and R. Corkish, J. Appl. Phys. **94**, 4930 (2003).

[31]P. P. Altermatt, F. Geelhaar, T. Trupke, X. Dai, A. Neisser, and E. Daub, Appl. Phys. Lett. **88**, 261901 (2006).

[32]T. Trupke, R. A. Bardos, and M. D. Abbott, Appl. Phys. Lett. **87**, 184102 (2005).

[33]K. R. McIntosh, J.-H. Guo, M. D. Abbott, and R. A. Bardos, Prog. Photovoltaics **16**, 279 (2008).

[34]J. A. Giesecke, T. Niewelt, M. Rüdiger, M. Rauer, M. C. Schubert, and W. Warta, Sol. Energy Mater. Sol. Cells **102**, 220 (2012).

[35]H. Kampwerth, S. Rein, and S. W. Glunz, in *Proceedings of the 3rd World Conference on Photovoltaic Energy Conversion, Osaka, Japan* (WCPEC-3 Organizing Committee, 2003), p. 1073.

[36]W. Kern and D. Puotinen, RCA Rev. **31**, 187 (1970).

[37]D. E. Kane and R. M. Swanson, in *Proceedings of the 18th IEEE Photovoltaic Specialists Conference, Las Vegas, NV* (IEEE, New York, USA, 1985), p. 578.

[38]D. K. Schroder, *Semiconductor Material and Device Characterization* (John Wiley & Sons, New York, 1990).

[39]R. A. Sinton and A. Cuevas, Appl. Phys. Lett. **69**, 2510 (1996).

[40]F. Dannhäuser, Solid-State Electron. **15**, 1371 (1972).

[41]J. Krausse, Solid-State Electron. **15**, 1377 (1972).

[42]G. Masetti, M. Severi, and S. Solmi, IEEE Trans. Electron Devices **30**, 764 (1983).

[43]D. B. M. Klaassen, Solid-State Electron. **35**, 953 (1992).

[44]In this work $(\mu_{\mathrm{n}} + \mu_{\mathrm{p}})$ is modeled with an empirical fit of the measured data of Refs. 40 and 41, as implemented in the data analysis sheet of the lifetime tester WCT-120. For carrier concentrations $<4 \times 10^{16}$ cm^{-3} as measured in this work, this fit is in good agreement with the mobility model of Ref. 43.

[45]H. W. Curtis and R. L. Verkuil, in *Lifetime Factors in Silicon, San Diego, CA, 1979* (American Society for Testing and Materials, Philadelphia, 1980), p. 211.

[46]H. Nagel, C. Berge, and A. G. Aberle, J. Appl. Phys. **86**, 6218 (1999).

[47]B. Hoex, J. Schmidt, P. Pohl, M. C. M. van de Sanden, and W. M. M. Kessels, J. Appl. Phys. **104**, 044903 (2008).

[48]T. Trupke, R. A. Bardos, F. Hudert, P. Würfel, J. Zhao, A. Wang, and M. A. Green, in *Proceedings of the 19th European Photovoltaic Solar Energy Conference, Paris, France* (WIP, Munich, Germany, 2004), p. 758.

[49]P. P. Altermatt, F. Geelhaar, T. Trupke, X. Dai, A. Neisser, and E. Daub, in *Proceedings of the 5th International Conference on Numerical Simulation of Optoelectronic Devices, Berlin, Germany* (IEEE, New York, USA, 2005), p. 47.

[50]T. Trupke, J. Appl. Phys. **100**, 063531 (2006).

[51]M. Rüdiger, T. Trupke, P. Würfel, T. Roth, and S. W. Glunz, Appl. Phys. Lett. **92**, 222112 (2008).

[52]E. Yablonovitch, D. L. Allara, C. C. Chang, T. Gmitter, and T. B. Bright, Phys. Rev. Lett. **57**, 249 (1986).

[53]A. B. Sproul, J. Appl. Phys. **76**, 2851 (1994).

[54]R. N. Hall, Phys. Rev. **87**, 387 (1952).

[55]W. Shockley and W. T. Read, Jr., Phys. Rev. **87**, 835 (1952).

[56]Even in high-quality FZ silicon a certain amount of such impurities might remain.

[57]A. A. Istratov, H. Hieslmair, and E. R. Weber, Appl. Phys. A **70**, 489 (2000).

[58]S. W. Glunz, S. Rein, J. Y. Lee, and W. Warta, J. Appl. Phys. **90**, 2397 (2001).

[59]J. Schmidt and K. Bothe, Phys. Rev. B **69**, 024107 (2004).

[60]A. A. Istratov, H. Hieslmair, and E. R. Weber, Appl. Phys. A **69**, 13 (1999).

[61]K. Bothe, R. Sinton, and J. Schmidt, Prog. Photovoltaics **13**, 287 (2005).

[62]D. Macdonald, T. Roth, P. N. K. Deenapanray, T. Trupke, and R. A. Bardos, Appl. Phys. Lett. **89**, 142107 (2006).

[63]D. Macdonald, J. Tan, and T. Trupke, J. Appl. Phys. **103**, 073710 (2008).

[64]M. J. Kerr and A. Cuevas, Semicond. Sci. Technol. **17**, 166 (2002).

[65]J. Schmidt and A. G. Aberle, J. Appl. Phys. **85**, 3626 (1999).

[66]R. Hezel and K. Jaeger, J. Electrochem. Soc. **136**, 518 (1989).

[67]B. Hoex, J. J. H. Gielis, M. C. M. van de Sanden, and W. M. M. Kessels, J. Appl. Phys. **104**, 113703 (2008).

[68]A. Richter, J. Benick, M. Hermle, and S. W. Glunz, Phys. Status Solidi RRL **5-6**, 202 (2011).

[69]F. Werner, B. Veith, D. Zielke, L. Kühnemund, C. Tegenkamp, M. Seibt, R. Brendel, and J. Schmidt, J. Appl. Phys. **109**, 113701 (2011).

[70]S. Steingrube, P. P. Altermatt, D. Zielke, F. Werner, J. Schmidt, and R. Brendel, in *Proceedings of the 25th European Photovoltaic Solar Energy Conference, Valencia, Spain* (WIP, Munich, Germany; and ETA, Florence, Italy, 2010), p. 1748.

[71]T. F. Ciszek and T. H. Wang, in *Proceedings of the 14th European Photovoltaic Solar Energy Conference, Barcelona, Spain* (H S Stephens & Associates, Bedford, UK, 1997), p. 103.

[72]J. del Alamo, S. Swirhun, and R. M. Swanson, Tech. Dig. Int. Electron Devices Meet. December **85**, 290 (1985).

[73]G. Dingemans, R. Seguin, P. Engelhart, M. C. M. van den Sanden, and W. M. M. Kessels, Phys. Status Solidi RRL **4**, 10 (2010).

[74]R. Häcker and A. Hangleiter, J. Appl. Phys. **75**, 7570 (1994).

[75]M. J. Kerr and A. Cuevas, Semicond. Sci. Technol. **17**, 35 (2002).

[76]To extract a unique low-injection Auger lifetime such a constant value is required as the application of the SRH formalism would lead to a strong correlation of the low-injection Auger lifetime with the low-injection SRH lifetime.

[77]S. Dauwe, J. Schmidt, A. Metz, and R. Hezel, in *Proceedings of the 29th IEEE Photovoltaics Specialists Conference, New Orleans, LA* (WIP, Munich, Germany; and ETA, Florence, Italy, 2002), p. 162.

[78]P. P. Altermatt, A. Schenk, F. Geelhaar, and G. Heiser, J. Appl. Phys. **93**, 1598 (2003).

[79]K. Misiakos and D. Tsamakis, J. Appl. Phys. **74**, 3293 (1993).

[80]A. Schenk, J. Appl. Phys. **84**, 3684 (1998).

[81]The single defect SRH recombination was modeled with the lifetime parameters $\tau_n = 3.0 \times 10^{-2}$ s and $\tau_p = 2.1 \times 10^{-2}$ s, and a defect energy level $E_t = 0.43$ eV from the conduction band edge.